Applied Thermal Engineering 123 (2017) 471–484

Contents lists available at ScienceDirect

Applied Thermal Engineering

journal homepage: www.elsevier.com/locate/apthermeng

Research Paper

Numerical simulation and optimization of heat transfer enhancement in a heat exchanger tube fitted with vortex rod inserts

Nianben Zheng, Peng Liu, Xinting Wang, Feng Shan, Zhichun Liu, Wei Liu *

School of Energy and Power Engineering, Huazhong University of Science and Technology, Wuhan 430074, China

HIGHLIGHTS

- Thermal-hydraulic performance in a heat exchanger tube with vortex rods is analyzed.
- Multi-objective optimization is conducted using CFD, ANN and NSGA-II.
- The optimal combination of design variables is obtained.

ARTICLE INFO

Article history:
Received 19 November 2016
Revised 19 May 2017
Accepted 21 May 2017
Available online 25 May 2017

Keywords:
Heat transfer enhancement
Vortex rod
Multi-objective optimization

ABSTRACT

In this work, numerical simulations have been performed to examine the thermal-hydraulic performance in a heat exchanger tube with vortex rod inserts. Analysis of flow characteristics and parametric study is carried out firstly. The results show that multiple vortices have been induced, and the parameters considered, i.e., vortex rod inclination angle (α), diameter ratio (d^*) and Reynolds number (Re) have a significant effect on the heat transfer and friction factor characteristics in the tube with vortex rods. To achieve the best configuration for the maximum heat transfer enhancement with the minimum pressure drop considering the interactive effects of the parameters. Multi-objective optimization together with artificial neural network has been implemented to search the optimal Pareto front. To evaluate the amount of heat transfer enhancement against pressure drop augmentation, a thermal-hydraulic performance evaluation parameter has been applied, and it is found that the vortex rod with $d^* = 0.058$ and $\alpha = 57.057°$ at $Re = 426.767$ gives the best thermal-hydraulic performance.

1. Introduction

With the increasing demands for efficient and compact heat exchangers, investigations of heat transfer enhancement techniques have received significant attention in the past few decades. Generally, heat transfer enhancement techniques can be classified into active methods, passive methods and compound methods. The passive methods are preferred because they require no external power input compared to the other methods. Among various passive methods available, tube inserts or turbulators have gained wide popularity in thermal engineering applications since they give scope of retrofitting existing devices and improving their thermal-hydraulic performance.

Tube inserts such as twisted tapes [1–10], coiled wires [11–13] and helical-screw tapes [14,15] have been commonly used in heat exchangers. Naphon [1] performed experimental investigations on the heat transfer and pressure drop behaviors in the double pipes with twisted tapes. The results showed that both the heat transfer rate and pressure drop in pipes with twisted tapes were enhanced significantly. Chang et al. [2] invented the broken twisted tape for heat transfer enhancement. According to their results, the heat transfer coefficients and friction factors of broken twisted tapes were 1.28–2.4 and 2–4.7 times over the smooth twisted tape, respectively. Numerical simulations of heat transfer and flow characteristics in a tube fitted with loose-fit twisted tape were presented by Eiamsa-ard et al. [3]. Later, Eiamsa-ard and his co-workers investigated many modified twisted tapes such as serrated twisted tape [4], delta-winglet twisted tape [5] and helically twisted tape [6]. Effects of perforated twisted tapes on thermal-hydraulic performance in a tube were explored by Bhuiya et al. [7]. They found that heat transfer rate and friction factor were about 110–340% and 110–360% higher than those of a smooth tube, respectively. Li et al. [8] numerically determined the effects of centrally hollow narrow twisted tapes on heat transfer enhancement. Promvonge [9] examined the thermal performance of quadruple V-finned twisted tapes experimentally. Vashistha et al. [10] experimentally studied the effects of multiple twisted tape

* Corresponding author.
E-mail address: w_liu@hust.edu.cn (W. Liu).

http://dx.doi.org/10.1016/j.applthermaleng.2017.05.112
1359-4311/

Nomenclature

ANN	artificial neural network
D	diameter of tube [m]
d^*	vortex rod diameter ratio
E	length of vortex rods [m]
e_{max}	maximum error
L	length of tube [m]
MSE	Mean Square Error
MOGA	multi-objective genetic algorithm
PIV	particle image velocimetry
p	pitch of vortex rods [m]
R	regression
R_0	tube radius [m]

Greek symbols

α	vortex rods inclination angle [°]
ρ	fluid density [kg m^{-3}]
μ	dynamic viscosity [kg m^{-1} s^{-1}]

Subscripts

in	inlet
i, j	Cartesian coordinates
m	mean
out	outlet
w	wall

inserts on the heat transfer and frictional losses. It was found that the maximum enhancement in heat transfer and pressure drop was 2.42 and 6.96 times that of a smooth tube. San et al. [11] measured the heat transfer and flow data in circular tubes fitted with coiled-wire inserts. Effects of ribbed and grooved wire coils on the thermal performance were experimentally examined by Chang et al. [12]. Akhavan-Behabadi et al. [13] experimentally investigated the heat transfer and flow characteristics of nanofluid flow inside a tube with wire coil inserts. Their results showed that heat transfer coefficient was raised up to 85%, while the pressure drop was increased by 475%. Guo et al. [14] numerically studied the heat transfer and fluid flow performance of tubes with helical screw-tape inserts. *CFD* investigations on heat transfer and flow characteristics of a tube with helical screw-tape without core-rod inserts were performed by Zhang et al. [15]

Some new types of tube inserts have been released by some researchers recently. Thermal-hydraulic characteristics in a tube fitted with twisted conical inserts were investigated numerically by Pourramezan and Ajam [16]. The results showed that twisted conical strip inserts caused additional swirl and turbulence in the flow, and the maximum Nusselt number ratio was 3.5, and the maximum friction factor ratio was 25. Tu et al. [17] numerically examined the thermal-hydraulic behaviors of turbulent flow in a heat exchanger tube with small pipe inserts. A novel wavy strip insert was proposed by Zhu et al. [18] for heat transfer enhancement of laminar flow in a round pipe. Skullong et al. [19] introduced the staggered-winglet perforated-tapes (*WPT*) to enhance the thermal performance in a round tube. According to their results, *WPT* provided heat transfer enhancement and pressure drop up to 2.4–4.7 and 5.1–42.9 times, respectively. Chingtuaythong et al. [20] reported the heat transfer and flow characteristics in a tube fitted with V-shaped rings. They found that V-shaped rings enhanced the thermal performance up to 5.8 times that of a smooth tube whereas the pressure drop was up to 82 times.

Above cited papers show that heat transfer can be enhanced with the utilization of tube inserts, but the pressure drop penalty is increased dramatically as well. Too much pressure drop penalty will impair the thermal-hydraulic performance inevitably. Therefore, achieving the maximum heat transfer enhancement with the minimum pressure drop penalty is crucial for the wide application of tube inserts. To solve the complex heat transfer and flow problems with conflicting objectives, some researchers [21–27] have adopted the multi-objective optimization method, which has been proven to be very efficient.

In this work, we propose a novel tube insert (i.e., vortex rod) for potential heat transfer enhancement in the heat exchanger tubes. Analysis of flow characteristics and parametric study has been conducted by numerical simulations. Particle image velocimetry (PIV) experiments have been performed to verify the flow structures in the tube with vortex rods. To determine the best configuration for the maximum Nusselt number ratio with the minimum friction factor ratio, an attempt has also been made to optimize the geometric parameters and the flow condition in this study using artificial neural network (*ANN*) and multi-objective genetic algorithm (*MOGA*).

2. Physical model

Geometry of a heat exchanger tube with vortex rods is explicitly presented in Fig. 1. The computational domain has the length (*L*) of 0.5 m and the diameter (*D*) of 0.02 m. These vortex rods are uniformly mounted on three connecting rods and are inserted in the tube. To reduce the influence from connecting rods on the heat transfer and flow fields, the connecting rods are designed to be very small. In particular, the diameter of the connecting rods is 0.001 m. The vortex rod has the length (*E*) of 0.008 m and the pitch (*P*) of 0.02 m. To study the effects of the diameter (*d*) and inclination angle (α) of the vortex rod on the thermal-hydraulic performance, the simulation of present work was conducted under various diameter ratios ($d^* = d/D$) and inclination angles. Details of the geometric parameters are given in Table 1.

3. Numerical study

3.1. Governing equations and boundary conditions

In this work, water is considered as the working fluid. Also, the gravity effect and viscous dissipation are not considered. Based on above assumptions, the flow is assumed to be laminar and steady. Therefore, the governing equations for continuity, momentum and energy are given in the following forms:

$$\frac{\partial(\rho u_i)}{\partial x_i} = 0 \tag{1}$$

$$\frac{\partial}{\partial x_j}(\rho u_i u_j) = -\frac{\partial P}{\partial x_i} + \frac{\partial}{\partial x_j}\left[\mu\left(\frac{\partial u_i}{\partial x_j} + \frac{\partial u_j}{\partial x_i}\right)\right] \tag{2}$$

$$\frac{\partial}{\partial x_j}\left(\rho u_j C_p T - k\frac{\partial T}{\partial x_j}\right) = 0 \tag{3}$$

where ρ is the density of fluid, u_i is a mean component of velocity in the direction of x_i, P is the pressure, and μ is the dynamic viscosity of water; C_P is the specific heat and k is the thermal conductivity.

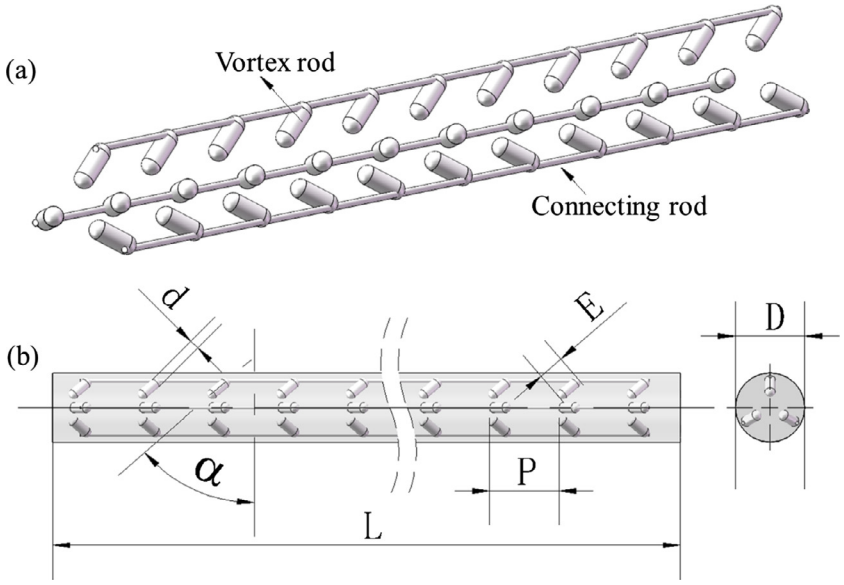

Fig. 1. Physical model: (a) vortex rods; (b) a tube with vortex rods.

Table 1
Geometric parameters of the tube and vortex rod.

L	D	E	p	α	$d^* = d/D$
0.5 m	0.02 m	0.008 m	0.02 m	15°, 30°, 45°, 60°, 75°	0.05, 0.10, 0.15, 0.20

At the inlet of the tube, the fully developed temperature and velocity profiles are specified using the user defined function (*UDF*). According to Ref. [28], the temperature and velocity profiles are given by Eqs. (4) and (5), respectively. The pressure-outlet condition is applied at the outlet. No-slip condition is assumed on the surface of tube wall and vortex rods. The tube wall is subjected to a uniform and constant heat flux of 2000 W m^{-2}.

$$T_{in} = T_c + \frac{qR_0}{k}\left[\left(\frac{r}{R_0}\right)^2 - \frac{1}{4}\left(\frac{r}{R_0}\right)^4\right] \tag{4}$$

$$u_{in} = u_c\left(1 - \frac{r^2}{R_0^2}\right) \tag{5}$$

where u_c is the velocity at the centerline of the tube, T_c is the temperature at the centerline of the tube. Also, q is the heat flux, R_0 is the tube radius, and r is the radial distance.

In this work, the Fluent 13.0 software was utilized to solve the governing equations. To handle the velocity-pressure coupling, the SIMPLE algorithm was applied. Second-order upwind scheme was chosen to discretize the convective terms. The convergence criterion was 10^{-6} for the continuity and momentum equations while 10^{-8} for the energy equation.

3.2. Parameter definition

The Reynolds number (Re) is defined as:

$$Re = \frac{\rho u D}{\mu} \tag{6}$$

where u is the mean flow velocity in the tube.

After computing the velocity and temperature fields, the average heat transfer coefficient (h) is calculated as follows:

$$h = \frac{q}{T_w - T_m} \tag{7}$$

where T_w is the wall temperature and T_m is the bulk temperature of water.

Nusselt number (Nu) is given by:

$$Nu = \frac{hD}{k} \tag{8}$$

The friction factor is given by:

$$f = \frac{\Delta P}{(L/D)\rho u^2/2} \tag{9}$$

where ΔP is the pressure drop across the computational domain.

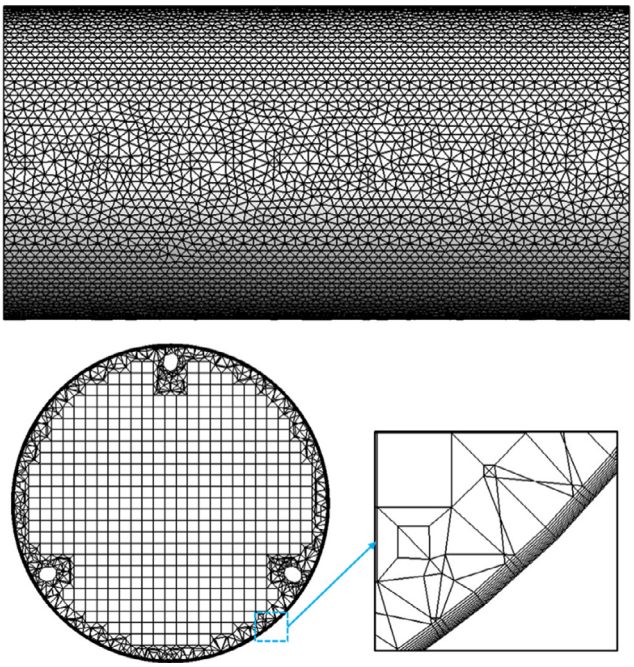

Fig. 2. Grid generation for a tube with vortex rods.

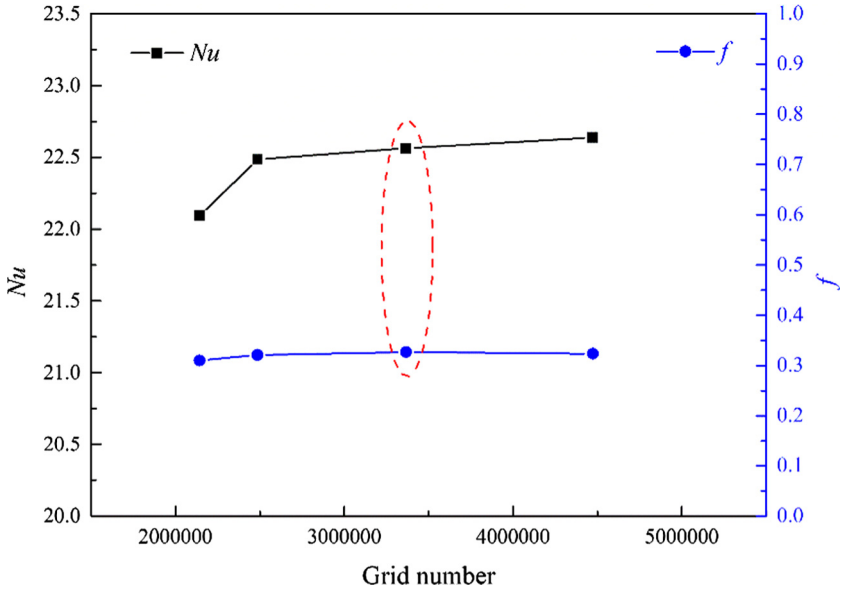

Fig. 3. The average *Nu* and *f* calculated by different grid systems with $d^* = 0.015$ and $\alpha = 45°$ at $Re = 1200$.

3.3. Grid generation and independence test

As shown in Fig. 2, the computational domain was discretized with hybrid grid consisting of prism grids, tetrahedral grids, hex core and pyramids by using ICEM CFD 13.0 software. In general, denser and finer grids lead to more accurate results. Therefore, four grid systems, with 2,143,696, 2,486,597, 3,366,230 and 4,473,182 elements, were used to conduct the grid independence test for vortex rod with $d^* = 0.015$ and $\alpha = 45°$ at $Re = 1200$. From Fig. 3, it is found that the relative deviation decreases with the increase of the grid number for both the Nusselt number and friction factor. Quantitatively, the relative deviations between the fine grid (3,366,230 elements) and the finest grid (4,473,182 elements) are 0.3% for the Nusselt number and 1.1% for friction factor, respectively, indicating that the fine grid system is dense enough. Therefore, we select the fine grid system with 3,366,230 elements for subsequent simulations.

3.4. Numerical method validation

Numerical simulations were, firstly, performed in a smooth tube to test the reliability of the present numerical method. The calculated results were compared with the experimental correlations [29]. According to Shah and London [29], the heat transfer and fluid friction correlations, i.e., Nu_0 (4.36) and f_0 (64/*Re*) were obtained for fully developed laminar flow in a smooth tube subject to constant surface heat flux condition. It should be noted that the numerical conditions were the same as those in the experiments. In particular, the fully developed temperature and velocity profiles were specified at the inlet to guarantee the fully developed laminar flow condition, and a uniform and constant heat flux of 2000 W m^{-2} was applied on the tube wall. Comparisons between numerical results and experimental correlations were shown in Fig. 4. It is clear that the numerical results agree well with the correlations, and the relative deviations are less than 4.7% and 4.8% for

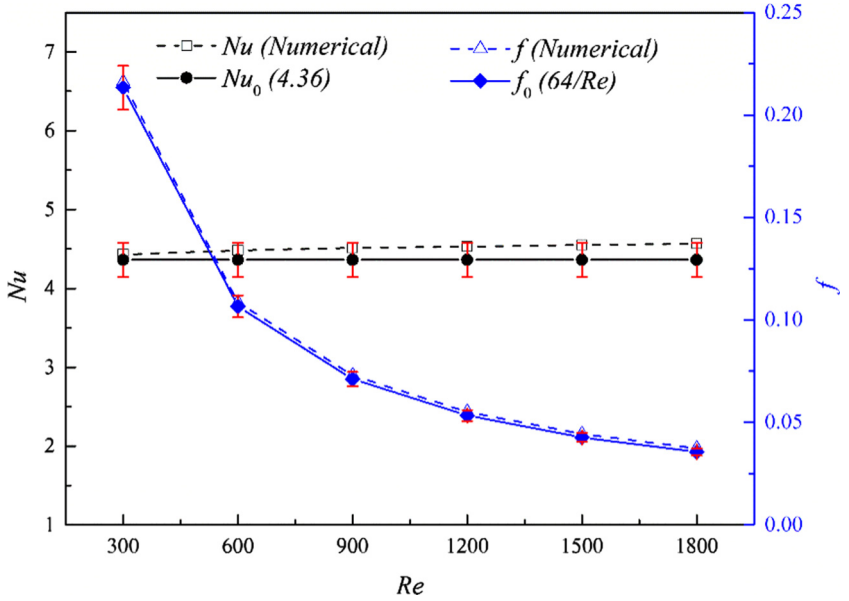

Fig. 4. Comparisons between numerical results and experimental correlations [29].

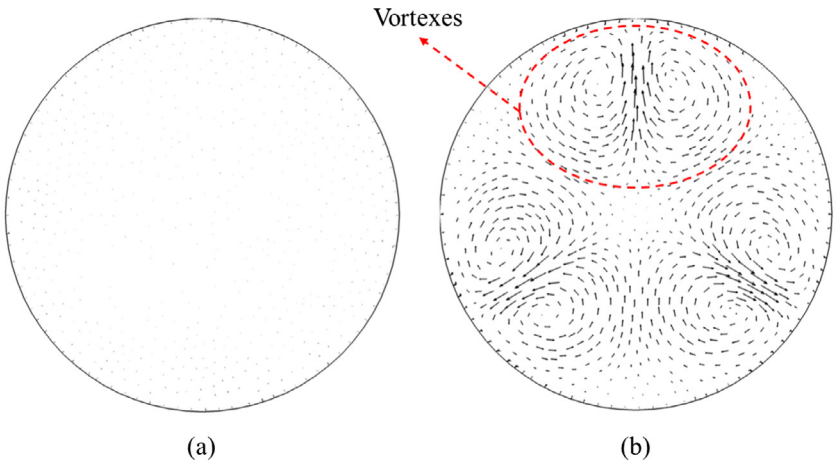

Fig. 5. Velocity vectors in the tubes: (a) the smooth tube; (b) the tube with vortex rods.

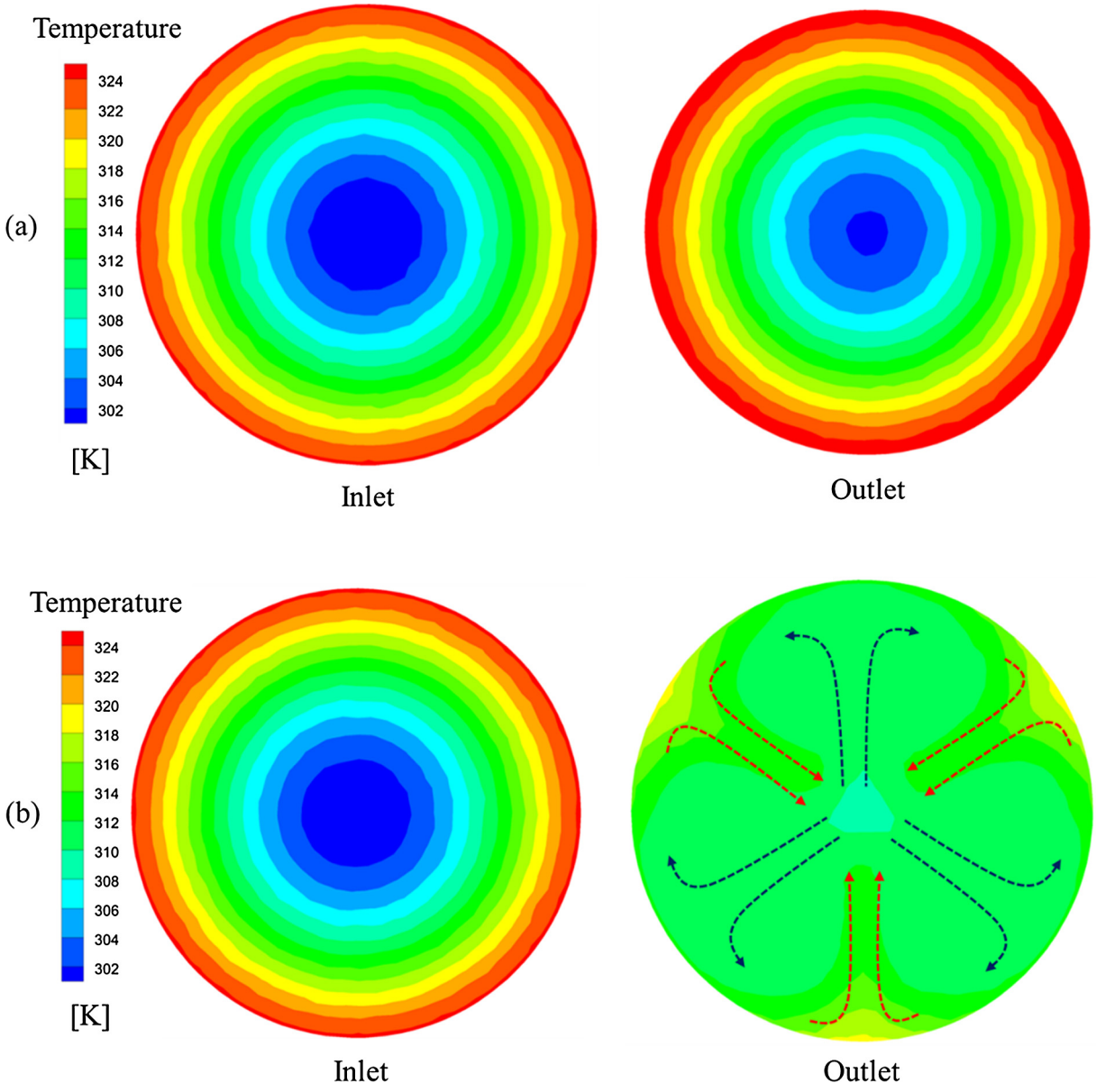

Fig. 6. Temperature contours at the inlet and outlet of the tubes: (a) the smooth tube; (b) the tube with vortex rods.

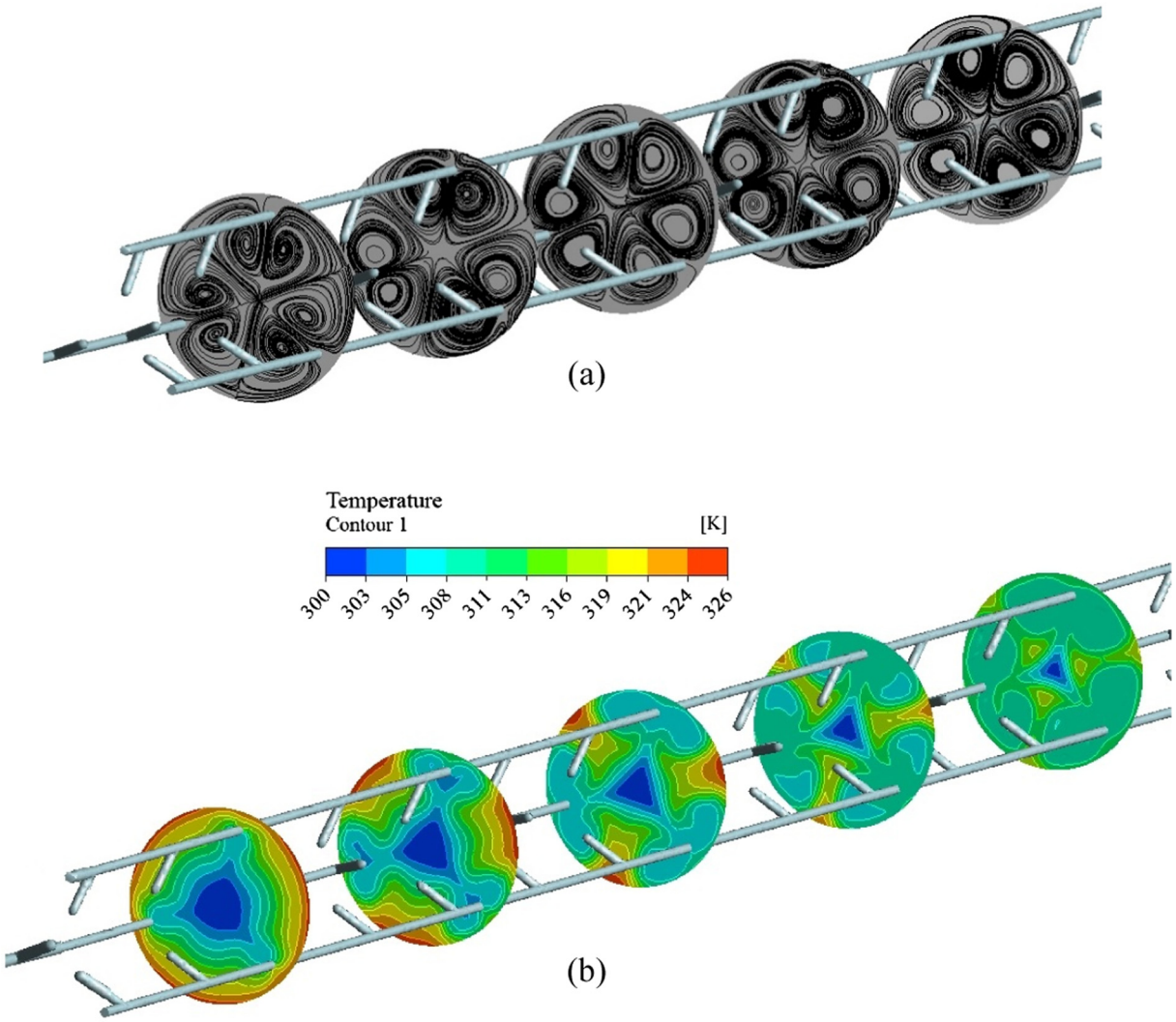

Fig. 7. Flow and temperature fields along the tube with vortex rods ($\alpha = 45°$, $d^* = 0.05$, $Re = 900$): (a) streamlines; (b) temperature distributions.

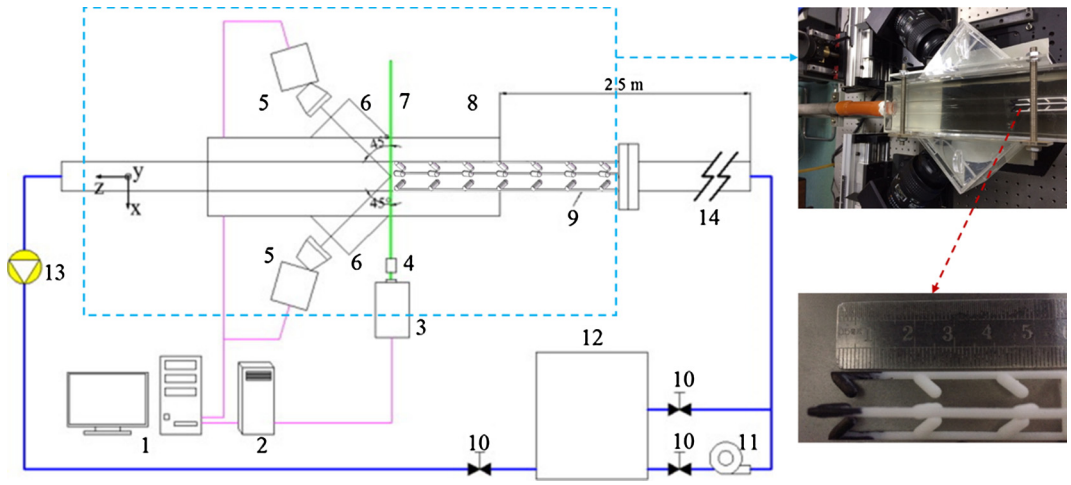

Fig. 8. Diagram of the experimental setup: 1. Personal computer, 2. Synchronizer, 3. Laser, 4. Lenses, 5. CCD camera, 6. Water prisms, 7. Laser light sheet, 8. Test section, 9. Vortex rods, 10. Control valves, 11. Water pump, 12. Water tank, 13. Electromagnetic flowmeter, 14. Calming section.

the Nusselt number and friction factor, respectively, indicating that the present numerical method is reliable.

4. Results and discussion

4.1. Flow structures and temperature distributions

In order to investigate the effect of vortex rods on the flow patterns, velocity vectors in the smooth tube and enhanced tube have been presented in Fig. 5. It is observed from Fig. 5 that multiple vortices have been induced in the enhanced tube, while no vortex is generated in the smooth tube. Vortices generated by the vortex rods are uniformly distributed in the tube. These vortices result in intense fluid mixing in the tube that fluid is transported towards the tube wall from the core flow region and fluid near the tube wall is injected towards the core flow region. Therefore, vortex rods have a significant effect on the flow pattern in the tube, and the flow pattern induced will affect the temperature distributions as well.

Fig. 6(a) and (b) shows the temperature distributions at the inlet and outlet of the smooth tube and the enhanced tube, respectively. It is evident that the temperature distributions are the same at the inlets for both tubes, while those at the outlets are quite different. To be more specific, the fluid temperature is much higher near the wall, while the fluid temperature is still very low in the core flow region of the smooth tube as plotted in Fig. 6(a). The large temperature difference implies that fluid, especially in the core flow region cannot get fully heated. From Fig. 6(b), it is clear that the temperature is much more uniformly distributed in the enhanced tube compared to that in the smooth tube, which can be related to the flow pattern generated by the vortex rods that cold fluid is transported towards the tube wall, and hot fluid near the wall is injected into the core flow region. This kind of fluid mixing can create large temperature gradients near the wall resulting in high heat transfer rate. Therefore, fluid in the tube with vortex rods can be fully heated, and uniform temperature distributions are achieved.

To further understand the physical mechanism for heat transfer enhancement in the tube with vortex rods. The streamlines and temperature distributions in transverse planes along the tube fitted with vortex rods are shown in Fig. 7(a) and (b), respectively. From Fig. 7(a), one sees that multiple vortices are induced in different transverse planes, indicating that multiple vortices have been generated in the whole flow region besides the outlet. These vortices result in strong fluid mixing along the tube, and the influence of these vortices on the temperature fields has been presented in Fig. 7(b). It is clear the fluid near the wall has very high temperature while the temperature of fluid in the core flow region is relatively low at the entrance. Because of the repeated fluid mixing induced by the multiple vortices along the tube, the low temperature regions decrease gradually, and the average temperature of the fluid increases progressively. As a result, the uniformity of the temperature field increases gradually along the tube.

4.2. Verification of the numerical results

The analyses above indicate that vortex rods have a significant effect on the flow structures in the tube, and the multiple vortices are the main flow characteristics in the tube with vortex rods. To verify the flow structures, we have setup the particle image velocimetry (PIV) experiments to measure the velocities. The experimental setup is shown in Fig. 8. The experimental system consists of three parts, which are (1) PIV measurement system; (2) water supply; (3) data acquisition and analysis system. The flow field measurements are conducted using the American TSI Stereo-PIV System. In the experiments, the POWERVIEW™ Plus 4MP cameras with 2048 × 2048 pixel resolution are used to capture the images, and the 532 nm Nd:YAG laser with lenses is applied to generate the light sheet. The hollow glass spheres with the diameter of 12 um are utilized as the seeding particles. In particular, the size of the interrogation window is 32 × 32 pixels with a 50% overlap, and 300 pairs of images are acquired for analysis using the INSIGHT 4G software. More details about the experimental setup can refer to [30].

Because of the occlusion problem caused by the connecting rods, the flow field measurements in the transverse plane can be performed only at the outlet of the tube. Fig. 9 shows the comparison of the experimental and numerical results in the tube with vortex rods ($\alpha = 45°$, $d^* = 0.05$, $Re = 600$). It is apparent that the velocity vector distributions measured by PIV experiments agree well with those obtained by numerical simulations. The main deviations occurs in the near wall regions, which can be attributed to the strong reflection of the tube wall that makes it difficult for the measurements. In addition, it is clear that multiple vortices are the main flow characteristics in the measured flow fields, which verifies the flow structures obtained by numerical simulations. Therefore, it can be concluded that the numerical model used in this work is reliable.

4.3. Parametric study

4.3.1. Effects of vortex rod inclination angle

The influence of vortex rod inclination angle on the Nusselt number ratio related to heat transfer enhancement and friction factor ratio related to pressure drop augmentation is presented in Fig. 10. It is found from Fig. 10(a) that Nusselt number ratios

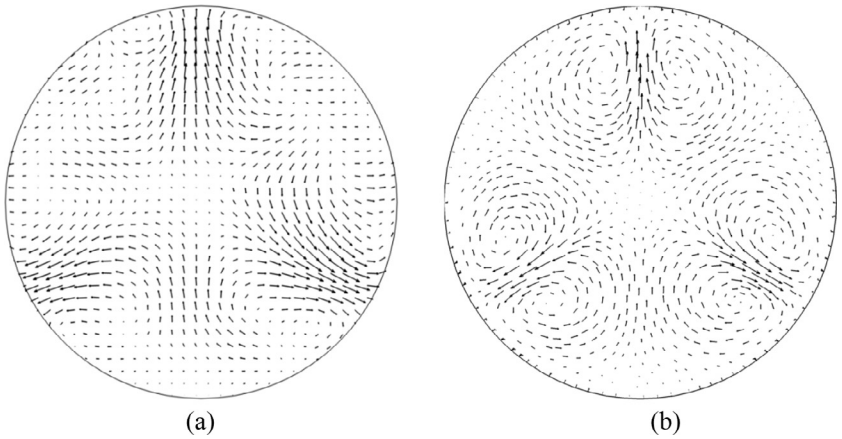

Fig. 9. Comparison of the velocity vectors in the tube with vortex rods ($\alpha = 45°$, $d^* = 0.05$, $Re = 600$): (a) PIV experiment; (b) Numerical simulation.

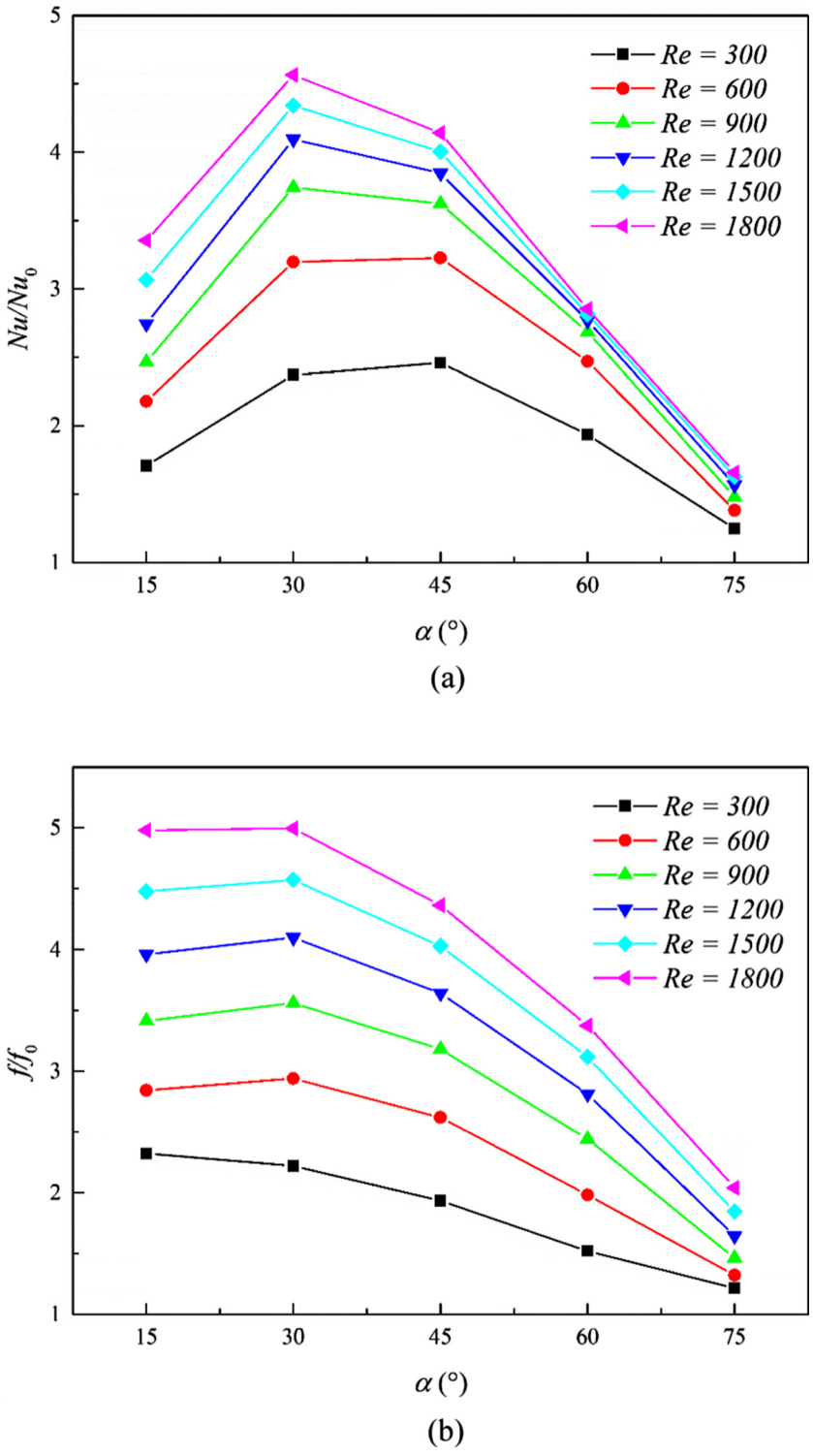

Fig. 10. Variations of Nu/Nu_0 and f/f_0 with vortex rod inclination angle for different Reynolds numbers at $d^* = 0.05$: (a) Nu/Nu_0; (b) f/f_0.

are more than one for all the cases investigated, indicating that vortex rods can enhance the heat transfer performance, and the enhancement over the smooth tube can be ascribed to the multiple vortices flow pattern. Additionally, Nusselt number ratios increase with the rise of the inclination angle from 15° to 30°, but a decreasing trend is found with the further increase of the inclination angle from 30° to 75° when $Re > 600$. The similar phenomenon is also observed at low Reynolds number ($Re \leq 600$), but the difference of Nusselt number ratios between the cases of $\alpha = 30°$ and $\alpha = 45°$ is quite small. The maximum Nusselt number ratio with the value of 8.01 is achieved at $\alpha = 30°$ and $Re = 1800$.

Fig. 10(b) illustrates the variation of the friction factor ratios with different inclination angles. It is clear that the friction factor ratios are much higher at small inclination angle ($\alpha = 15°$ and $\alpha = 30°$). With the further increase of the inclination angle ($\alpha \geq 30°$), a sharp decreasing trend of friction factor ratio is found, implying that larger inclination angles are preferred for the cases where pressure drop is strictly limited.

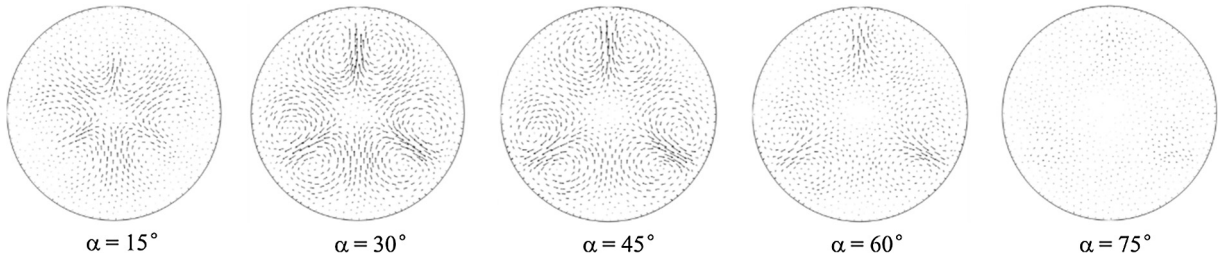

Fig. 11. Velocity vectors at the outlet of tubes with different vortex rod inclination angles.

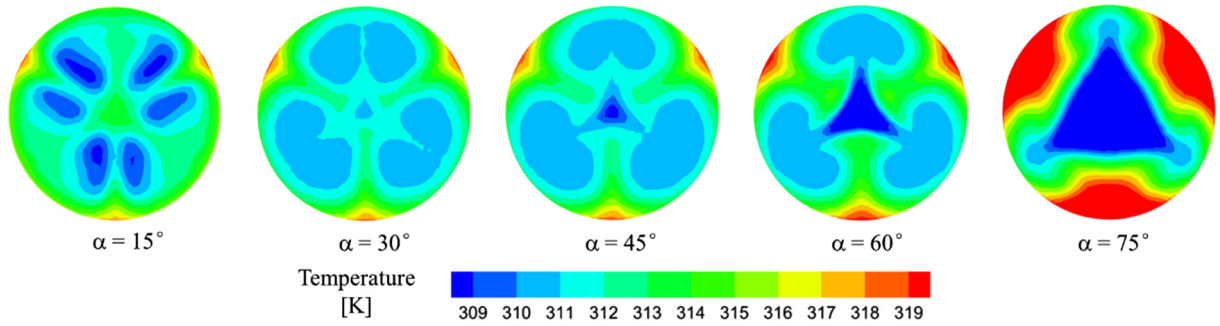

Fig. 12. Temperature distributions at the outlet of tubes with different vortex rod inclination angles.

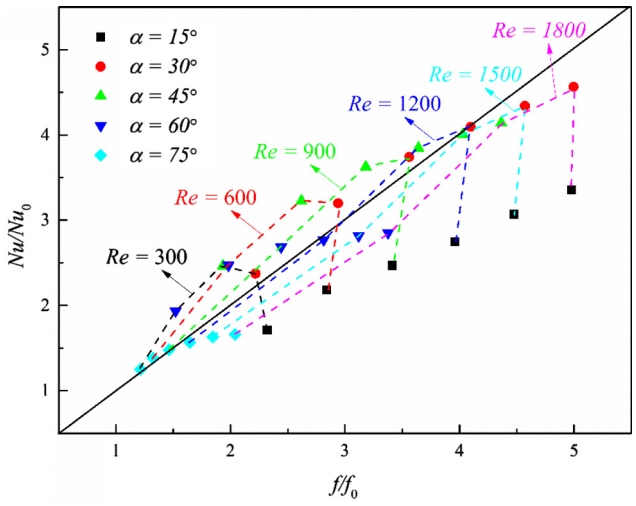

Fig. 13. Variation of Nu/Nu_0 with f/f_0.

To further understand the effect of inclination angle on the heat transfer and flow performance, velocity vectors and temperature distributions at the outlet of the tubes have also been illustrated in Figs. 11 and 12, respectively. It is evident from Fig. 11 that multiple vortices are induced in all the cases. The strength of vortices increases with an increase of the inclination angle, and reaches the maximum at $\alpha = 30°$. With the further increase of the inclination angle, the strength of vortices tends to decrease. From Fig. 12, it is found that the fluid temperature is more uniformly distributed in the tube with higher strength of vortices. This can be explained by the fact that stronger vortices lead to better fluid mixing, which creates larger temperature gradients near the wall leading to higher heat transfer performance. It should be noted that strong vortices or secondary flow will impair the velocity in the axial flow direction leading to more pressure drop penalty.

Fig. 13 shows the variation of Nu/Nu_0 with f/f_0 in the enhanced tubes of different inclination angles. One sees that the range of Nusselt number ratios is similar to that of the friction factor ratio. Except for the cases of $\alpha = 15°$ that the Nusselt number ratios are lower than the friction factor ratios for all the Reynolds numbers, the Nusselt number ratios tend to be larger than the friction factor ratios in the cases with lower Reynolds numbers, which can be ascribed to the compound effects of vortex rod inclination angle and Reynolds number.

4.3.2. Effects of vortex rod diameter ratio

Variations of Nu/Nu_0 with f/f_0 with different vortex rod diameter ratios at $\alpha = 30°$ have been shown in Fig. 14(a) and (b), respectively. The variation trend of Nusselt number ratios is similar to that of friction factor ratios. Both of them increase with the increasing Reynolds number at a given vortex rod diameter ratio. In addition, both Nu/Nu_0 and f/f_0 increase with an increase of vortex rod diameter ratio for a given Reynolds number, indicating that larger vortex rod diameter ratio leads to better heat transfer performance, but the expense is more flow blockages caused by the vortex rods.

Velocity vectors at the outlet of tubes with different vortex rod diameter ratios have been compared in Fig. 15. It shows that multiple vortices are generated in the tube with different vortex rod diameter ratios, and the strength of vortices is considered highest for the case of $d^* = 0.20$, followed by the case of $d^* = 0.15$, and $d^* = 0.10$, the case of $d^* = 0.05$ is the lowest. With the increase of the strength of vortices, fluid can get better mixed in the tube that more uniformity of temperature and larger average temperature is achieved, as shown in Fig. 16. It should be pointed out that the larger vortex rod diameter ratio will cause more flow blockages leading to more pressure drop though the faster heat transfer rate is obtained at the same time.

The variation of Nu/Nu_0 with f/f_0 for different vortex rod diameter ratios and Reynolds numbers is presented in Fig. 17. One sees that Nusselt number ratios are larger than the friction factor only for the cases with smaller vortex rod diameter ratio ($d^* = 0.05$ and $d^* = 0.10$) at low Reynolds numbers. As to the other cases, the Nusselt number ratios are smaller than the friction factor. Therefore, it is can be concluded that the growth rate of friction factor ratios is faster than that of the Nusselt number ratios,

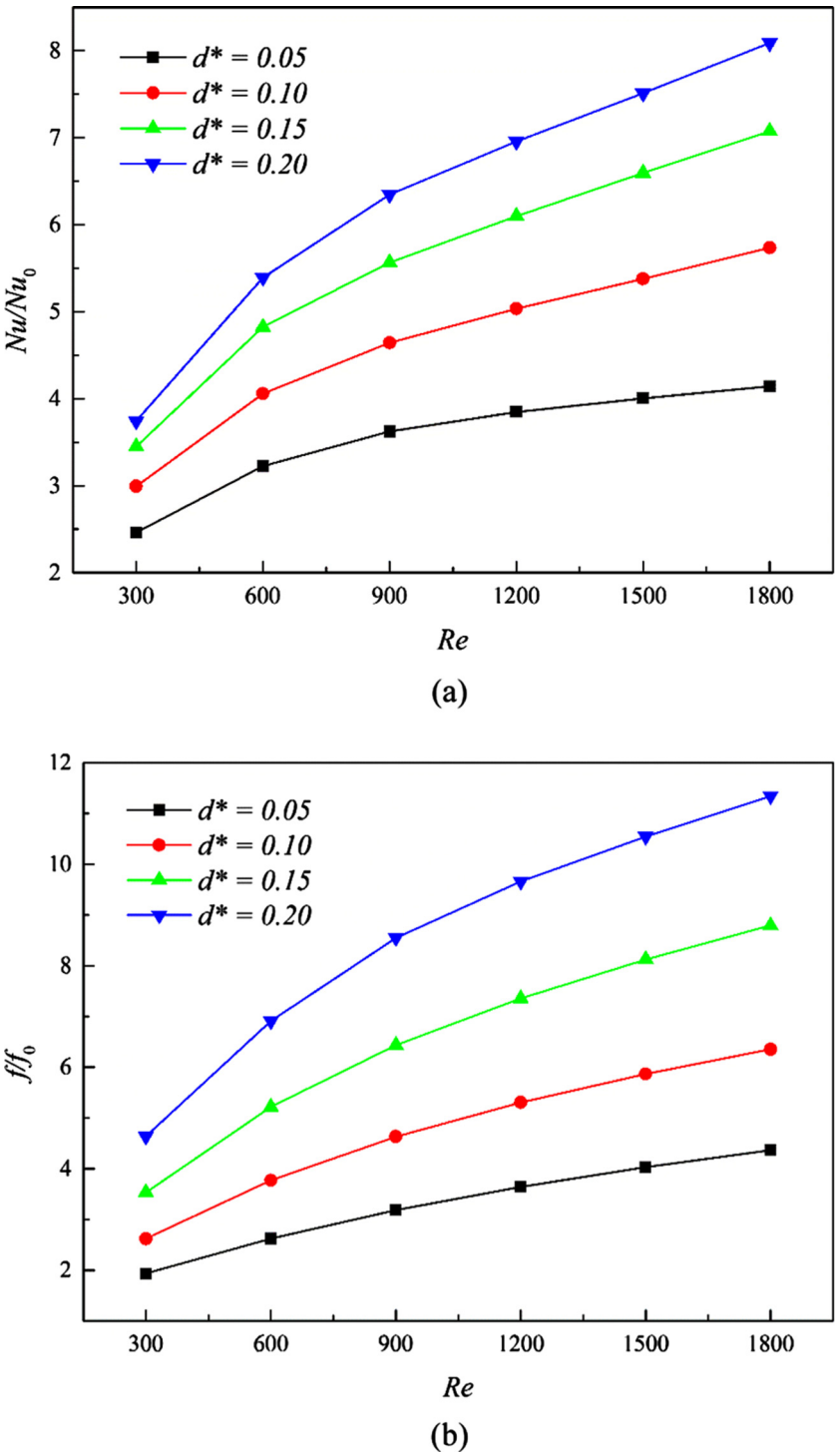

Fig. 14. Variations of Nu/Nu_0 and f/f_0 with different vortex rod diameter ratios at $\alpha = 30°$: (a) Nu/Nu_0; (b) f/f_0.

implying that the influence of vortex rod diameter ratio on the friction factor ratio is more significant compared to the Nusselt number ratio.

4.4. Optimization study

4.4.1. Overview

In the above parametric study, the effect of a single parameter on the thermal-hydraulic performance is considered at a time while the compound effects of the parameters are not taken into consideration. As a result, achieving the optimum configuration for heat transfer enhancement is not possible just based on the results of the above parametric study. Since the present problem has two conflicting objectives. One of the objectives, which is related to heat transfer performance, is the Nusselt number ratio Nu/Nu_0, where Nu_0 is the Nusselt number in the smooth tube. The other objective related to flow performance is the friction factor ratio f/f_0, where f_0 is the friction factor in the smooth tube. So, to obtain the optimal thermal-hydraulic performance in a heat exchanger tube fitted with vortex rods, it is necessary to carry out a multi-objective optimization to determine the best possible design points. The flowchart for optimization is presented in Fig. 18.

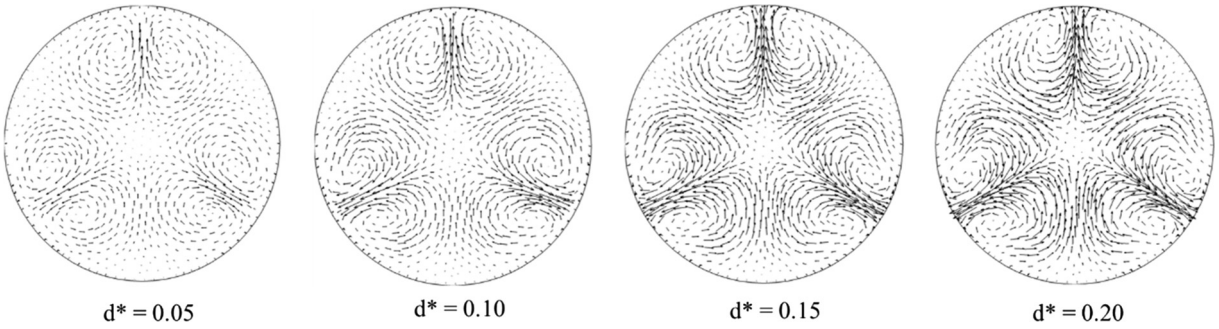

Fig. 15. Velocity vectors at the outlet of tubes with different vortex rod diameter ratios.

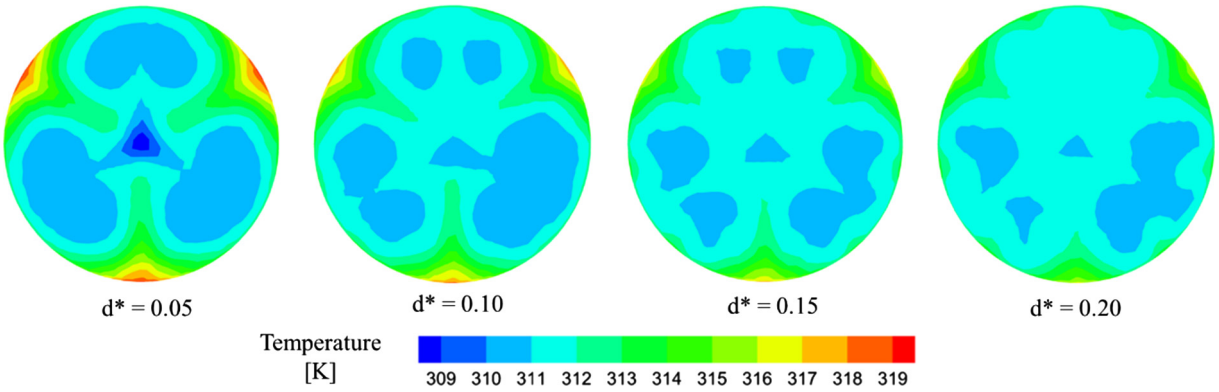

Fig. 16. Temperature distributions at the outlet of tubes with different vortex rod diameter ratios.

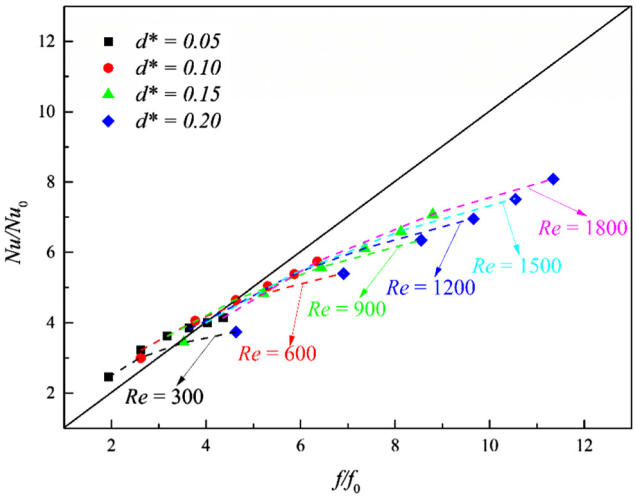

Fig. 17. Variation of Nu/Nu_0 with f/f_0.

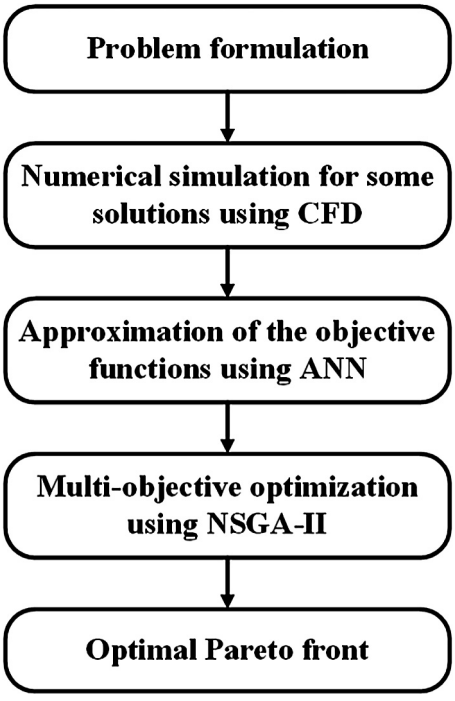

Fig. 18. The flowchart for optimization.

4.4.2. Artificial neural networks results

As shown in Fig. 18, prior to performing the multi-objective optimization, the relationship between the inputs and outputs should be estimated. In this study, we use a two-layer feed-forward artificial neural network (*ANN*) which has sigmoid hidden neurons and linear output neurons as shown in Fig. 19. *ANN* trains the network by a training process to appropriate values without understanding the physical mechanisms. Thus, *ANN* is a rapid surrogate to obtain the objective functions. In detail, data created from numerical simulations were divided into to three groups. 70% of the data were used to train the network with the Levenberg-Marquardt back propagation algorithm; 15% of the data were used to measure network generalization, and the remaining data were used to test the network. The default performance functions for the feed-forward network are Mean Square Error (*MSE*)

$$MSE = \frac{1}{n}\sum_{i=1}^{n}\left(X_{i,ANN} - X_{i,Num}\right)^2$$

$$R = \sqrt{1 - \sum_{i=1}^{n}\frac{\left(X_{i,ANN} - X_{i,Num}\right)^2}{X_{i,Num}^2}}$$

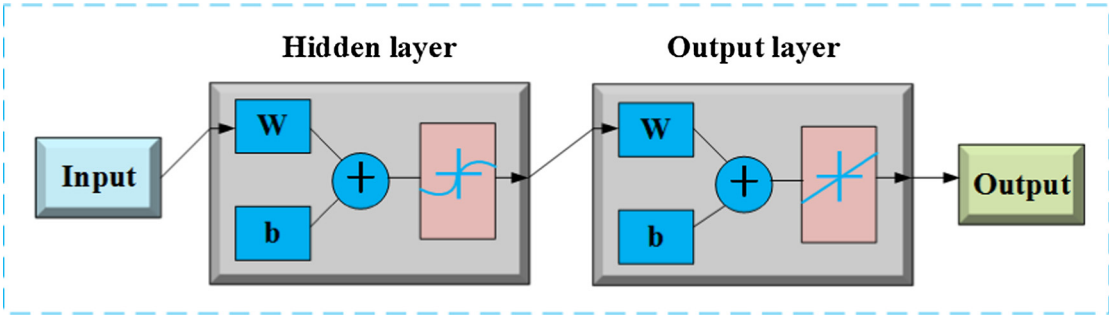

Fig. 19. Schematic of neural network.

and Regression (R). Definitions of *MSE* and Regression are given as follows:

$$MSE = \frac{1}{n}\sum_{i=1}^{n}\left(X_{i,ANN} - X_{i,Num}\right)^2 \tag{10}$$

$$R = \sqrt{1 - \sum_{i=1}^{n}\frac{\left(X_{i,ANN} - X_{i,Num}\right)^2}{X_{i,Num}^2}} \tag{11}$$

To select appropriate number of neurons in the hidden layer, a neuron independence test was carried out. Table 2 shows the results of neuron independence test. The number of neurons varies from 1 to 20. Comparison of the *MSE* and R values of different numbers of neurons shows that 12 and 14 neurons lead to the minimum *MSE* and the maximum R for the approximation of Nusselt number ratios and friction factor ratios, respectively. Therefore, these two numbers of neurons are selected in the hidden layer of the network.

4.4.3. Multi-objective optimization results

The multi-objective problem for the present problem can be expressed as follows:

$$\begin{aligned} &\text{Minimization} \quad f(d^*, \alpha, Re) = [-Nu/Nu_0, f/f_0] \\ &\text{Subjected to} \quad 0.05 \le d^* \le 0.20 \\ &\qquad\qquad\quad 15^\circ \le \alpha \le 75^\circ \\ &\qquad\qquad\quad 300 \le Re \le 1800 \end{aligned}$$

Two geometric parameters namely, the rod diameter ratio (d^*) and the rod inclination angle (α), and the Reynolds number (Re) were chosen as the design variables for optimization. The range of the design variables and the selected values are shown in Table 3.

To optimize the conflicting objective functions approximated by *ANNs* simultaneously, and determine the optimal Pareto front, the commonly used fast non-dominated sorting genetic algorithm (NSGA-II) is applied. Details of the NSGA-II method and procedures to search the optimal Pareto front can be found in Ref. [31]. It should be noted that NSGA-II was implemented in MATLAB using the *gamutliobj* toolbox. Table 4 shows the parameter setting for NSGA-II.

Table 2
Neuron independence test.

Number of neurons	$-Nu/Nu_0$		f/f_0	
	MSE	R	*MSE*	R
1	0.8322	0.87288	0.1879	0.97925
2	0.2391	0.9672	0.3607	0.98258
3	0.0744	0.9847	0.0168	0.99851
4	0.088	0.99144	0.0527	0.9982
5	0.1539	0.98118	0.0573	0.99681
6	0.0259	0.99526	0.0216	0.99882
7	0.0591	0.98976	0.0342	0.99902
8	0.0791	0.99291	0.0666	0.99874
9	0.0205	0.99815	0.0329	0.99873
10	0.0284	0.99865	0.0453	0.99898
11	0.0226	0.99733	0.0222	0.99965
12	**0.0112**	**0.9993**	0.0431	0.99913
13	0.0146	0.99863	0.0203	0.99953
14	0.0253	0.99845	**0.0185**	**0.99972**
15	0.0144	0.99893	0.0347	0.99934
16	0.0448	0.99816	0.0277	0.99956
17	0.031	0.99561	0.0402	0.9994
18	0.0165	0.99833	0.0399	0.99911
19	0.0219	0.99864	0.0232	0.99953
20	0.0154	0.99724	0.0379	0.99945

Table 3
The range of the design variables and the selected values.

Design variables	Lower bound	Upper bound	Selected values
d^*	0.05	0.20	0.05, 0.10, 0.15, 0.20
α (°)	15	75	15, 30, 45, 60, 75
Re	300	1800	300, 600, 900, 1200, 1500, 1800

Table 4
Parameter setting for NSGA-II.

Parameter	Value setting
Population size	100
Pareto front population fraction	0.7
Crossover fraction	0.8
Generation	500
Functional tolerance	10^{-6}

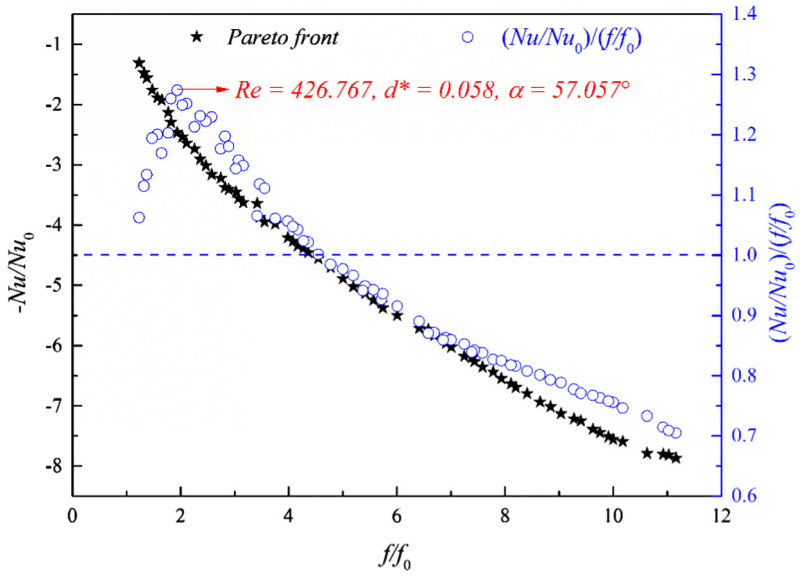

Fig. 20. Pareto front for Nu/Nu_0 and f/f_0.

The optimal Pareto front searched by NSGA-II has been shown in Fig. 20. All the points in the optimal Pareto front are optimal points that these points have no dominancy over one another. If we move from one optimal point to another, one objective function will improve, and the other objective function will decrease. To search the optimal design variables for practical applications, we use a thermal-hydraulic performance evaluation parameter, $(Nu/Nu_0)/(f/f_0)$, to evaluate the amount of heat transfer enhancement against pressure drop augmentation. The corresponding value of $(Nu/Nu_0)/(f/f_0)$ with respect to each optimal point in the optimal Pareto front has also been plotted in Fig. 18. These points are marked by blue circles. As the figure indicated, the values of $(Nu/Nu_0)/(f/f_0)$ are above unity as the friction factor ratio is lower than 4.5. The maximum value of $(Nu/Nu_0)/(f/f_0)$ is found to be 1.27 achieved at $Re = 426.767$, $d^* = 0.058$ and $\alpha = 57.057°$. Therefore, this combination of design variables is recommended for industrial applications.

5. Conclusions

In this work, numerical simulations were performed to examine the thermal-hydraulic performance in a tube with vortex rods at first. Then, multi-objective optimization of the design variables namely, d^*, α and Re for the maximum heat transfer enhancement with the minimum pressure drop was implemented using the combination of *ANN* and NSGA-II. It was concluded as follows:

1. The presence of vortex rods changes the flow structures in the tube that multiple vortices are generated. The multiple vortices have been verified by PIV experiments. Because of vortex motions, cold fluid is transported towards the tube wall and hot fluid near the wall is injected into the core flow region. This kind of fluid mixing can create large temperature gradients near the wall resulting in high heat transfer performance.
2. In the range of study, Nusselt number ratios tend to be larger than friction factor ratios in the cases with larger inclination angles and lower diameter ratios at low Reynolds numbers.
3. According to the results of optimization, the best thermal–hydraulic performance for vortex rods is obtained with $d^* = 0.058$ and $\alpha = 57.057°$ at $Re = 426.767$. This combination of design variables for vortex rods is recommended for industrial applications.

Acknowledgments

The work was supported by the National Key Basic Research Program of China (973 Program) (2013CB228302) and the National Natural Science Foundation of China (51376069, 51606073).

References

[1] P. Naphon, Heat transfer and pressure drop in the horizontal double pipes with and without twisted tape insert, Int. Commun. Heat Mass Transf. 33 (2006) 166–175.
[2] S.W. Chang, T.L. Yang, J.S. Liou, Heat transfer and pressure drop in tube with broken twisted tape insert, Exp. Thermal Fluid Sci. 32 (2007) 489–501.
[3] S. Eiamsa-ard, K. Wongcharee, S. Sripattanapipat, 3-D numerical simulation of swirling flow and convective heat transfer in a circular tube induced by means of loose-fit twisted tapes, Int. Commun. Heat Mass Transf. 36 (2009) 947–955.
[4] S. Eiamsa-ard, P. Promvonge, Thermal characteristics in round tube fitted with serrated twisted tape, Appl. Therm. Eng. 30 (2010) 1673–1682.
[5] S. Eiamsa-ard, K. Wongcharee, P. Eiamsa-ard, C. Thianpong, Heat transfer enhancement in a tube using delta-winglet twisted tape inserts, Appl. Therm. Eng. 30 (2010) 310–318.
[6] S. Eiamsa-ard, K. Yongsiri, K. Nanan, C. Thianpong, Heat transfer augmentation by helically twisted tapes as swirl and turbulence promoters, Chem. Eng. Process. 60 (2012) 42–48.
[7] M.M.K. Bhuiya, M.S.U. Chowdhury, M. Saha, M.T. Islam, Heat transfer and friction factor characteristics in turbulent flow through a tube fitted with perforated twisted tape inserts, Int. Commun. Heat Mass Transf. 46 (2013) 49–57.
[8] P. Li, Z. Liu, W. Liu, G. Chen, Numerical study on heat transfer enhancement characteristics of tube inserted with centrally hollow narrow twisted tapes, Int. J. Heat Mass Transf. 88 (2015) 481–491.
[9] P. Promvonge, Thermal performance in square-duct heat exchanger with quadruple V-finned twisted tapes, Appl. Therm. Eng. 91 (2015) 298–307.
[10] C. Vashistha, A.K. Patil, M. Kumar, Experimental investigation of heat transfer and pressure drop in a circular tube with multiple inserts, Appl. Therm. Eng. 96 (2016) 117–129.
[11] J.-Y. San, W.-C. Huang, C.-A. Chen, Experimental investigation on heat transfer and fluid friction correlations for circular tubes with coiled-wire inserts, Int. Commun. Heat Mass Transf. 65 (2015) 8–14.
[12] S.W. Chang, J.Y. Gao, H.L. Shih, Thermal performances of turbulent tubular flows enhanced by ribbed and grooved wire coils, Int. J. Heat Mass Transf. 90 (2015) 1109–1124.
[13] M.A. Akhavan-Behabadi, M. Shahidi, M.R. Aligoodarz, An experimental study on heat transfer and pressure drop of MWCNT–water nano-fluid inside horizontal coiled wire inserted tube, Int. Commun. Heat Mass Transf. 63 (2015) 62–72.
[14] J. Guo, M. Xu, L. Cheng, Numerical investigations of circular tube fitted with helical screw-tape inserts from the viewpoint of field synergy principle, Chem. Eng. Process. 49 (2010) 410–417.

[15] X. Zhang, Z. Liu, W. Liu, Numerical studies on heat transfer and friction factor characteristics of a tube fitted with helical screw-tape without core-rod inserts, Int. J. Heat Mass Transf. 60 (2013) 490–498.
[16] M. Pourramezan, H. Ajam, Modeling for thermal augmentation of turbulent flow in a circular tube fitted with twisted conical strip inserts, Appl. Therm. Eng. 105 (2016) 509–518.
[17] W. Tu, Y. Wang, Y. Tang, A numerical study on thermal-hydraulic characteristics of turbulent flow through a circular tube fitted with pipe inserts, Appl. Therm. Eng. 101 (2016) 413–421.
[18] X.W. Zhu, Y.H. Fu, J.Q. Zhao, A novel wavy-tape insert configuration for pipe heat transfer augmentation, Energy Convers. Manage. 127 (2016) 140–148.
[19] S. Skullong, P. Promvonge, C. Thianpong, M. Pimsarn, Heat transfer and turbulent flow friction in a round tube with staggered-winglet perforated-tapes, Int. J. Heat Mass Transf. 95 (2016) 230–242.
[20] W. Chingtuaythong, P. Promvonge, C. Thianpong, M. Pimsarn, Heat transfer characterization in a tubular heat exchanger with V-shaped rings, Appl. Therm. Eng. 110 (2017) 1164–1171.
[21] M.-A. Moon, K.-Y. Kim, Analysis and optimization of fan-shaped pin–fin in a rectangular cooling channel, Int. J. Heat Mass Transf. 72 (2014) 148–162.
[22] H. Safikhani, A. Abbassi, A. Khalkhali, M. Kalteh, Multi-objective optimization of nanofluid flow in flat tubes using CFD, artificial neural networks and genetic algorithms, Adv. Powder Technol. 25 (2014) 1608–1617.
[23] A. Abdollahi, M. Shams, Optimization of shape and angle of attack of winglet vortex generator in a rectangular channel for heat transfer enhancement, Appl. Therm. Eng. 81 (2015) 376–387.
[24] A. Abdollahi, M. Shams, Optimization of heat transfer enhancement of nanofluid in a channel with winglet vortex generator, Appl. Therm. Eng. 91 (2015) 1116–1126.
[25] R.S. Jadhav, C. Balaji, Fluid flow and heat transfer characteristics of a vertical channel with detached pin-fin arrays arranged in staggered manner on two opposite endwalls, Int. J. Therm. Sci. 105 (2016) 57–74.
[26] H. Alimoradi, M. Shams, Optimization of subcooled flow boiling in a vertical pipe by using artificial neural network and multi objective genetic algorithm, Appl. Therm. Eng. 111 (2017) 1039–1051.
[27] M. Darvish Damavandi, M. Forouzanmehr, H. Safikhani, Modeling and Pareto based multi-objective optimization of wavy fin-and-elliptical tube heat exchangers using CFD and NSGA-II algorithm, Appl. Therm. Eng. 111 (2017) 325–339.
[28] J. Holman, Heat Transfer, ninth ed., McGraw-Hill Inc, Boston, New York, 2002, pp. 168–169.
[29] R.K. Shah, A.L. London, Laminar Flow Forced Convection in Ducts: A Source Book for Compact Heat Exchanger Analytical Data, Academic Press, 1978.
[30] P. Liu, N. Zheng, F. Shan, Z. Liu, W. Liu, Numerical study on characteristics of heat transfer and friction factor in a circular tube with central slant rods, Int. J. Heat Mass Transf. 99 (2016) 268–282.
[31] K. Deb, A. Pratap, S. Agarwal, T. Meyarivan, A fast and elitist multiobjective genetic algorithm: NSGA-II, IEEE Trans. Evolut. Comput. 6 (2002) 182–197.